**Article:**
Nguyen, HT, Hensel, A and Goycoolea, FM (2022) Chitosan/cyclodextrin surface-adsorbed naringenin-loaded nanocapsules enhance bacterial quorum quenching and anti-biofilm activities. Colloids and Surfaces B: Biointerfaces, 211. 112281. ISSN 0927-7765

https://doi.org/10.1016/j.colsurfb.2021.112281

# Chitosan/cyclodextrin surface-adsorbed naringenin-loaded nanocapsules enhance bacterial quorum quenching and anti-biofilm activities

**Hao Thanh Nguyen[1,4], Andreas Hensel[2], Francisco M. Goycoolea[3,4*]**

[1] Faculty of Biotechnology, Vietnam National University of Agriculture, 100000 Hanoi, Vietnam

[2] Institute for Pharmaceutical Biology and Phytochemistry, University of Münster, Germany

[3] School of Food Science and Nutrition, University of Leeds, Leeds, United Kingdom

[4] Institute for Biology and Biotechnology of Plants, University of Münster, Germany

* Correspondence: F.M.Goycoolea@leeds.ac.uk; Tel.: +44(0)-113-343-1412

**Abstract**: Pathogenic bacteria use quorum sensing (QS), a cell-to-cell communication process that uses small signalling molecules, to regulate several essential virulence factors such as bioluminescence, biofilm formation, and bacterial motility. Naringenin, a bitter and colourless flavanone ubiquitous in herbs and fruits, has been shown to inhibit QS activity in *P. aeruginosa* by decreasing the production of pyocyanin and elastase. In this study, to evaluate the anti-QS activity of naringenin against an *E. coli* Top 10 biosensor, we developed a novel system using β-cyclodextrin (Captisol®) surface-adsorbed nanoformulations loaded with naringenin. The results showed that in both the nanocapsule (NC) and nanoemulsion (NE) formulations, the obtained colloidal particles have an appropriate size distribution and high association efficiency of naringenin, namely ~ 92.88 and ~ 67.98 %, respectively. These formulations remained stable for 24 h and showed a biphasic controlled release profile in bacterial M9 medium. Captisol® was effectively immobilized on the NC's surface, resulting in a surface charge inversion from positive (~ + 42mV) to negative (~ -32mV). The biosensor assay revealed that NC outperformed NE in quenching the QS response and the incorporation of naringenin at the NC's multifunctional surface enhanced this bioactivity. Cytotoxicity assays showed that when it was associated in NC, naringenin at a concentration of 188 μM was not cytotoxic to Caco2 cells, thus highlighting the cytoprotective effect of the developed formulation. Biofilm formation, a QS-mediated virulence factor, was inhibited up to ~ 60 % in naringenin-loaded NC (188 μM), indicating the synergistic effect of positively charged chitosan with the bioactivity of naringenin and the NC' advantageous high surface area-to-volume ratio.

**Keywords:** naringenin; chitosan; cyclodextrin; nanocapsules; quorum sensing; Escherichia coli Top 10

Number of words: 6305
Number of Figures: 7
Number of Tables: 1

## 1. Introduction

Overuse of antibiotics has led to a decrease in their efficacy to combat bacterial-mediated diseases. Antibiotic-resistant bacteria that are difficult or impossible to treat are causing a global health crisis, as bacteria have evolved to be able to bypass almost every antibiotic deployed [1–4]. New approaches to overcome this problem are urgently needed. On the one hand, new generations of effective antibiotics and vaccines are needed to keep pace with the huge demand. On the other, alternative innovative approaches to overcome bacterial multidrug resistance, must accompany these efforts. Rather than focusing on either bactericidal or bacteriostatic approaches, for decreasing resistance, it seems more strategic to target virulence factors that are required for infection and causing disease (e.g., toxin function and delivery, regulation of virulence expression and bacterial adhesion), while preserving the host's endogenous microbiome and impose fewer selective pressures on the pathogenic bacteria [1].

One such potential approach might be to interfere with quorum sensing (QS), a cell-to-cell communication process that bacteria use to communicate, whereby they coordinate and regulate gene expression and synchronize social behaviors in response to the cell density [5,6]. Diverse types of QS gene circuits are based either on the excretion and detection of, or response to, extracellular autoinducer signaling molecules, which act like hormones in higher organisms, to trigger the coordinated responses [7]. In many cases, autoinducers can elicit responses directly related to pathogenesis, such as the production of virulence factors (e.g., toxins and proteases), bioluminescence, swarming motility, and other immune-evasive factors [8,9], such as the production of biofilms. In a series of previous studies in our group [10–12], we have examined the inhibition of QS under different approaches using an *E. coli* Top 10 reporter strain that contains the "listening" genetic cassette of marine *Vibrio fisheri* responsible for the development of bioluminescence [13].

QS is not essential for the growth of bacteria, hence strategies that lead to inhibition of QS, also known as quorum quenching (QQ), would disarm virulence rather than killing bacteria, leading to weaken the selective pressure imposed on the pathogens and postpone the evolution of resistance to QQ drugs [14]. As such, QS appears to be a promising target for anti-virulence therapy [7]. If one could block the autoinducers' communication processes that coordinate these pathogenic behaviors, bacteria would, in principle, lose their ability to attack the host and thus would be less able to form organized structures that boost resistance to antibiotics. Different type of compounds have been mainly recovered from extracts of marine algae [15], terrestrial plants [16–18] and bacteria [14,19].

The use of different types of nanomaterial to deliver and enhancing the activity of QSIs has been recognized to open new possibilities to develop innovative biomaterials for bacterial anti-QS. A promising approach might be pairing these nanomaterial systems with different type of phytochemicals that have shown QSI activity (e.g. limonoids, kaempferol, quercetin, *trans*-

cinnamaldehyde) [18,20–23]. Although previous studies have reported that flavonoids' insufficient solubility and poor dissolution has hampered their chemical stability and bioavailability [24], encapsulating them in biopolymer-based materials can improve their anti-virulence activity, as our group and others have shown for quercetin [10,12], *trans*-cinnamaldehyde [25] and other anti-virulent and antimicrobial agents [26,27]. This increase in activity might be attributed to enhanced bioavailability and/or prolonged release, where lower doses in encapsulated formulations are needed to overcome the resistance posed by physiological barriers as compared to free agents [28,29].

Flavanone naringenin (NAR) is a bitter and colorless flavanone that occurs in a variety of herbs and fruits, including grapefruit [30], sour orange [31], and water mint [32], etc. A recent study showed that NAR significantly reduced biofilm formation in *P. aeruginosa* (strain PAO1) by hindering the production of pyocyanin and elastase without affecting bacterial growth [22]. In a different study, Vikram *et al.* reported that in *V. harveyi*, NAR and other tested flavonoids (kaempferol, quercetin and apigenin) were effective antagonists of HAI-1 and AI-2-mediated cell–cell signalling, others autoinducers of QS [33]. Although promising, NAR suffers from low oral bioavailability, critically limiting its clinical potential; thus, approaches to enhance its bioavailability have been sought. Efforts to form inclusion complexes of NAR with hydroxypropyl-β-cyclodextrin revealed that the solubility of NAR was able to be increased over 400-fold [34]. Further, NAR-loaded nanoparticles have been found to have more potent antitumor effects than free NAR in preventing the formation of oral squamous cell carcinoma [35]. Other studies have shown that encapsulating NAR in chitosan nanoparticles enhanced its *in vitro* anticancer and antioxidant properties and its delivery [36].

In the present work, we aimed to design novel formulations of NAR-loaded nanocapsules and examined their anti-QS and anti-biofilm effects on an *E. coli* Top 10 AHL-regulated reporter strain. The comparison of the QS inhibition properties of the different type of formulations has helped to broaden our understanding of the role of the encapsulation strategies on the efficiency of delivery of the bioactive payload to bacterial cells and their cytoprotective effect in Caco-2 cells. We have gained proof of concept of the developed approach with the potential dual capacity to deliver anti-QS compounds such as naringenin, while concomitantly possibly quench AHL (3OC6-HSL) autoinducer by the adsorbed cyclodextrin, thus achieving a synergistic effect on the antivirulence response.

## 2. Materials and methods

### 2.1. Materials

Chitosan sample was of biomedical grade from Heppe Medical Chitosan GmbH (Halle/Saale, Germany), namely, sample Code HMC 70/5 (CAS 9012-76-04) Batch no. 212-170614-01 (degree of acetylation 32.4 % as determined by $^{1}$H NMR; $M_w$ ~ 29,267 g.mol$^{-1}$ and $M_n$ ~ 18,033 g.mol$^{-1}$ as determined by SEC-MALS-DRI-viscosity [37]). Soybean lecithin was from Cargill

(Epikuron 145 V, Cargill GmbH, Hamburg, Germany); Miglyol® 812N (Batch no. 151130), was donated by Sasol GmbH (Witten, Germany). Captisol® (sulphobutyl ether-β-cyclodextrin sodium salt; SBE-β-CD) was a kind gift from CyDex, Inc_USA. NAR, 3OC6HSL and the rest of chemicals were all analytical grade and purchased from Sigma-Aldrich (Hamburg, Germany).

2.2. Methods

2.2.1. Preparation of the nanoformulations

a) Nanocapsule (NC) and nanoemulsion (NE) formulations: the chitosan-coated nanocapsules were prepared according to the protocol developed by Calvo et al. with slight modifications [38]. Briefly, 5 mL of ethanolic organic phase containing 62.5 µL Miglyol 812 N, 20 mg lecithin and 18.75 mM NAR was immediately poured into 10 mL aqueous phase (0.5 mg/mL chitosan dissolved in 5% stoichiometric excess of HCl). The milky mixture was concentrated in a rotavapor (Büchi R-210, Büchi Labortechnik GmbH, Essen, Germany) at 40 °C until a final volume of one-third of the original was obtained (~ 5 mL) to yield a final NAR concentration of ~ 3.75 mM. The nanoemulsion (NE) formulation was prepared using the identical procedure, but miliQ water was used in the aqueous phase. Control (unloaded) NC and NE formulations were prepared that did not include NAR.

b) Captisol®-surface-adsorbed NC. These systems were obtained by harnessing the strong electrostatic interaction between the cationic polysaccharide surface of the chitosan-coated NC and the negatively charged Captisol®. For this purpose, we dissolved Captisol® in Milli-Q water at different concentrations (ranging from 0.19 to 25.64 mM). Afterwards, this aqueous solution was immediately mixed with unloaded or loaded NC (~1 mg/mL chitosan) and incubated for 1 h at room temperature. The volume ratio between NC and Captisol® was kept the same for all the experiments at 3:1 (v/v). Several formulations were prepared by altering the positive/negative charge ratio ($[NH_3^+]/[SO_3^-]$) defined by the equivalent amine group of chitosan and the sulfate group of Captisol®, respectively, ranging from 0.075 to 10.

2.2.2. Physicochemical characterization of nanocapsules

The Z-average particle sizes (hydrodynamic diameter) and size distributions (PDI) of the NC were determined by dynamic light scattering with non-invasive back scattering (DLS-NIBS) at 25 °C detected at an angle of 173° fitted with a red laser light output ($\lambda$ = 632.8 nm) using a Malvern Zetasizer Nano ZS instrument (ZEN3600, Malvern Instruments, UK). The zeta

potentials (ζ) was measured by phase analysis light scattering and mixed laser Doppler velocimetry (M3-PALS) at 25 °C using the same instrument. The samples were diluted 1:50 in 1 mM KCl before measurement.

2.2.3. Loading and association efficiency of nanocapsules

The freshly prepared nanoformulations were partitioned by ultracentrifugation at 16,000 rpm for 1 h at 15 °C using a Mikro 220R ultracentrifuge (Hettich GmbH & Co. KG, Tuttlingen, Germany). NAR's pellet in the subnatant (*i.e.*, insoluble crystalline NAR) was resuspended with absolute ethanol up to 1 mL before its absorbance at 289 nm was measured by UV spectrophotometer. The loading efficiency (LE %) was calculated as the percentage of entrapped NAR with respect to the total mass of nanocapsules. The association efficiency (AE %) was calculated as the difference between the total amount of NAR incorporated in the formulation and the amount present in the subnatant (Equation 1)

$$Association\ efficiency\ (\%) = \frac{[Total_{Drug}] - [Free_{Drug}]}{[Total_{Drug}]} \times 100 \quad (1)$$

2.2.4. Stability test

An aliquot of 50 µL of selected nanocapsule formulations were added to a sterile cuvette containing 950 of M9 medium previously equilibrated at 37 °C. The mixtures were incubated at standard conditions (37 °C, 48 h, agitation of 100 rpm). The Z-avergage size and PDI were measured as described above at different time points of 0, 30, 60, 120, 240, 360, 720 and 1440 min.

2.2.5. *In vitro* release studies

An aliquot of 800 µL of a NAR-loaded nanosystem was transferred to a dialysis tube (Pure-a-lyzer Maxi 0.1–3.0 ml, Mw cut-off = 6 kDa, Sigma-Aldrich GmbH, Steinheim, Germany) and placed in a sterile glass beaker with 79.2 mL of M9 medium previously equilibrated at 37 °C. At appropriate time points, an aliquot of 300 µL was withdrawn, replaced by fresh M9 medium. NAR content of the aliquots was determined by UV spectrophotometry at wavelength of 289 nm and was calculated by interpolation using a calibration curve.

2.2.6. TEM images

The ultrastructure of the nanocapsules was investigated by transmission electron microscopy (TEM) images, which were attained on a transmission electron microscope (Philips TEM

CM10, Eindhoven, Netherlands) fitted with a bottom-mounted camera TVIPS TEM Cam F416 and having an accelerating voltage of 80 kV. Briefly, specimens were prepared by mixing 10 µL of 1 % (w/v) uranyl acetate with an equal volume of nanocapsules previously diluted 1:10 with water for 30 seconds. Immediately afterwards, 10 µL of the solution-containing samples was placed onto a carbon-copper grid with a Formvar® film (200 mesh) for 30 seconds. Excess liquid was removed using filter paper, and the grids were then allowed to evaporate for at least 24 h in a desiccator.

2.2.7. Cell viability assay

The cytotoxicity of the nanoformulations and components was evaluated using the 3-[4,5-dimethylthiazol-2-yl]-2,5-diphenyltetrazolium bromide (MTT) assay [28,39] to determine mitochondrial dehydrogenase activity as a marker of cell viability. Briefly, $10^4$ cells/well were seeded in a 96-well plate in supplemented MEM medium. After 24h, the cells were washed twice with PBS before the sample was added (100 µL/well, n =8) and incubated for 24h. The samples were then removed and replaced with 100 µL MEM medium and 25 µL of MTT solution (5 mg/mL dissolved in PBS). After 2 h incubation at 37 °C, the medium and MTT solution were discarded and replaced by 100 µL DMSO to dissolve the formed dye. The absorbance was measured at $\lambda$ = 570 nm in a microplate reader (Safire, Tecan AG, Austria). Relative viability values were calculated by dividing individual viabilities by the mean of the negative control.

2.2.8. QS inhibition against *E. coli* Top10

QS assay was conducted as described previously [10]. Details of the protocol can be found in Supplementary Information.

2.2.9. Antibiofilm formation assay

Antibiofilm formation assay was performed as described by George A. O'Toole *et al*., [40] with slight modifications. Briefly, overnight bacterial culture of the *E. coli* Top10 in LB broth was diluted 1:100 into M9 fresh medium. 10 µL of the treatment formulations and 190 µL of the dilution were added to each well in a round-bottom 96-well plate and then incubated at 37 °C for 48 h without shaking. After incubation, loose cells were removed by turning the plate over and shaking out the liquid. Plates were carefully rinsed twice in a large beaker of water. After placing the microplate upside down on a paper towel for 1 h, adding 200 µL per well of 0.1 % crystal violet solution to stain the adhered cells. After 20 min, the excess stain was removed by

rinsing the plate 3-4 times with water in a large beaker as outlined above. 200 µL of 30 % acetic acid was added to each well, and the absorbance of the solubilized dye was measured at 590 nm using a Spectra Max-M2 Microplate Reader (Molecular Devices, US/Canada). For each experiment, background staining was corrected by subtracting the crystal violet bound to uninoculated controls from those of the samples. To estimate the antibiofilm activity (%) of a given treatment, the following relationship was used (Equation 2).

$$\text{Antibiofilm activity (\%)} = [1- (OD_{Testsample} - OD_{Blank})/(OD_{Untreated\ control} - OD_{Blank})] \times 100 \quad (2)$$

## 3. Results

### 3.1. Physicochemical properties

The physicochemical characteristics, encapsulation and loading efficiency of unloaded (blank) and NAR-loaded NC and NE are summarized in Table 1. The Z-average diameter of unloaded NC was ~147 nm, slightly greater than unloaded NE (Ø ~130 nm). Notably, when NAR was loaded at two different concentrations, namely 5 and 3.75 mM, this did not significantly influence the physicochemical characteristics of loaded NC or NE. Similar dimensions were observed in 5 mM NAR-loaded NC and NE, which were ~149 and ~ 134 nm, respectively. Overall, the polydispersity index (PDI) of all systems was very low, ranging from ~ 0.1 to ~ 0.2. As expected, both unloaded and NAR-loaded NC had strongly positive ζ of ~ +42 and ~ +40 mV, respectively. In contrast, unloaded NE and NAR-loaded NE, lacking the chitosan shell, possessed strongly negative ζ of ~ -54 and ~ -60 mV, respectively.

**Table 1.** Physicochemical characteristics, encapsulation efficiency (EE) and loading efficiency (LE) of blank and NAR-loaded nanocapsules and nanoemulsions.

| Nanoformulations Code[1] | Z-average size (d., nm) | Polydispersity index | ζ -potential (mV) | Encapsulation efficiency (%) | Loading efficiency (%) |
|---|---|---|---|---|---|
| $B_{NE}$ | 130 ± 4 | 0.133 | - 53.5 ± 3.12 | - | - |
| NAR $L_{NE}$ 5 mM | 134 ± 7 | 0.148 | - 61.3 ± 0.99 | 46.32 ± 2.17 | 3.82 ± 0.18 |
| NAR $L_{NE}$ 3.75 mM | 133 ± 4 | 0.166 | - 57.5 ± 4.35 | 67.98 ± 2.61 | 4.18 ± 0.16 |
| $B_{NC}$ | 147 ± 11 | 0.142 | + 41.6 ± 1.85 | - | - |
| NAR $L_{NC}$ 5 mM | 149 ± 7 | 0.105 | + 38.3 ± 2.31 | 82.05 ± 4.74 | 6.20 ± 0.36 |
| NAR $L_{NC}$ 3.75 mM | 142 ± 3 | 0.138 | + 40.4 ± 0.57 | 92.88 ± 3.19 | 5.32 ± 0.18 |

[1]$B_{NE}$: Blank nanoemulsions, $B_{NC}$: Blank nanocapsules, NAR: Naringenin, $L_{NE(NC)}$: Loaded nanoemulsion/ nanocapsules (followed by NAR's concentration)

The encapsulation efficiency (EE %) and loading efficiency (LE %) in loaded NC were significantly higher than in loaded NE at both 5 mM (82.05 *vs*. 46.32 %, respectively) and 3.75

mM (92.88 *vs*. 67.98 %, respectively). These results indicate that NC's chitosan shell promotes encapsulation of the lipophilic drug in the nanocarrier in keeping with previous studies in various payloads such as diazepam [38], docetaxel [41], capsaicin [28], *trans*-cinnamaldehyde [25], quercetin [12] .We found that decreasing the final amount of loaded drug from 5 to 3.75 mM significantly increased the EE in both loaded NC and loaded NE as observed in previous studies [25].

### 3.2. Stability of the nanosystems in bacterial M9 medium

Figure 1 shows the time-evolution average size and PDI measurements of both unloaded and 3.75 mM NAR-loaded NC and NE systems incubated in bacterial M9 medium. The size and PDI remained fairly constant for both types of systems during incubation for 24 h, in agreement with our previous studies [12,25,28,29] . The adsorption of different amounts of Captisol® onto the NCs' surface did not affect their colloidal stability.

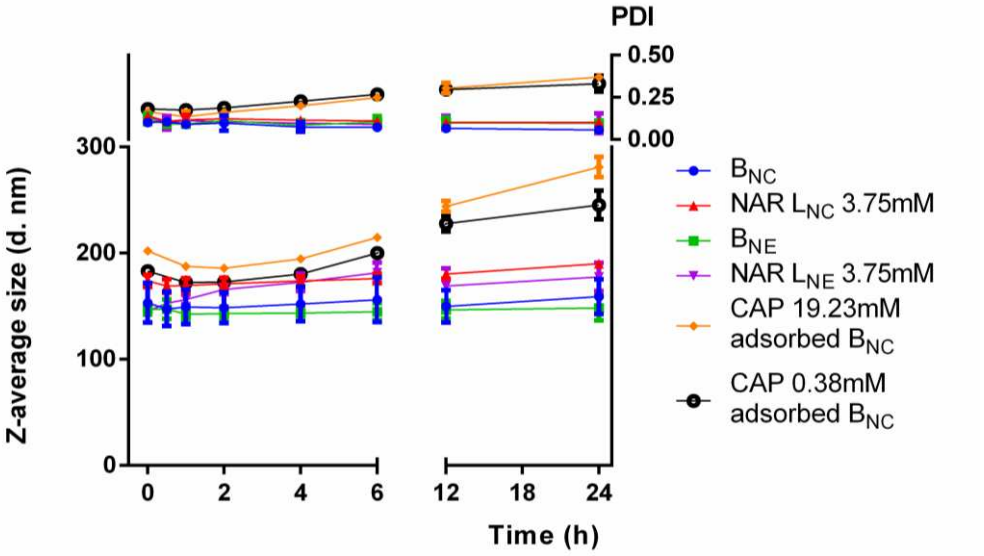


**Figure 1.** Time-evolution average diameter and average PDI of unloaded and loaded NC and NE systems during incubation in M9 medium (at 37 ºC) for 24 h. Data represent mean values ± SD ($n$ = 3).

### 3.3. Naringenin *in vitro* release studies in M9 medium

The results of the *in vitro* release studies are shown in Figure 2. The release rate was very slow and steady in the first 6 h, followed by an exponential release after 12 h; the total NAR release reached nearly 30 and 40 % for the NC and NE systems, respectively. The total payload release seemed to reach a plateau after 24 h for both systems. After 24 h, a greater percentage of NAR was released from NE (~ 55.19 %, ~ 1.125 mM), compared to that released from NC (~ 39.47 %, ~ 1.129 mM).

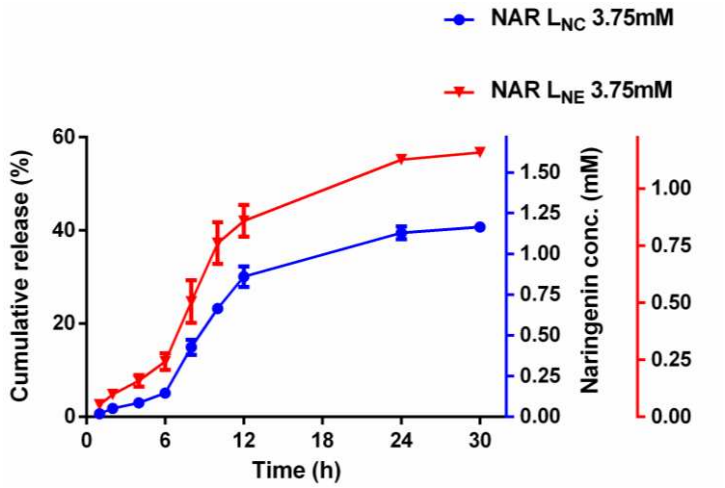


**Figure 2.** *In vitro* release of NAR in M9 medium (37 ºC, agitation 100 rpm) of 3.75 mM NAR-loaded (blue color y axis) nanocapsules (NAR $L_{NC}$) and (red color y axis) nanoemulsions (NAR $L_{NE}$).

### 3.4. Captisol® surface-adsorbed NC

Under the second pursued approach, we examined the feasibility to prepare a core-corona nanostructure compromised by an oil core NE (either blank or loaded with NAR) stabilized by a complex layer-by-layer (LbL)-type shell of lecithin, chitosan and Captisol® to enhance the anti-QS effect of nanoparticle systems. To this end, either $B_{NC}$ or NAR $L_{NC}$3.75 mM were first prepared, and then Captisol® was associated by electrostatic adsorption onto their polymeric surfaces. The Z-average size, PDI and ζ parameters are shown in Figure 3 and Figure S1 and S2. The detail characteristic of the system was described in supplementary 2.1

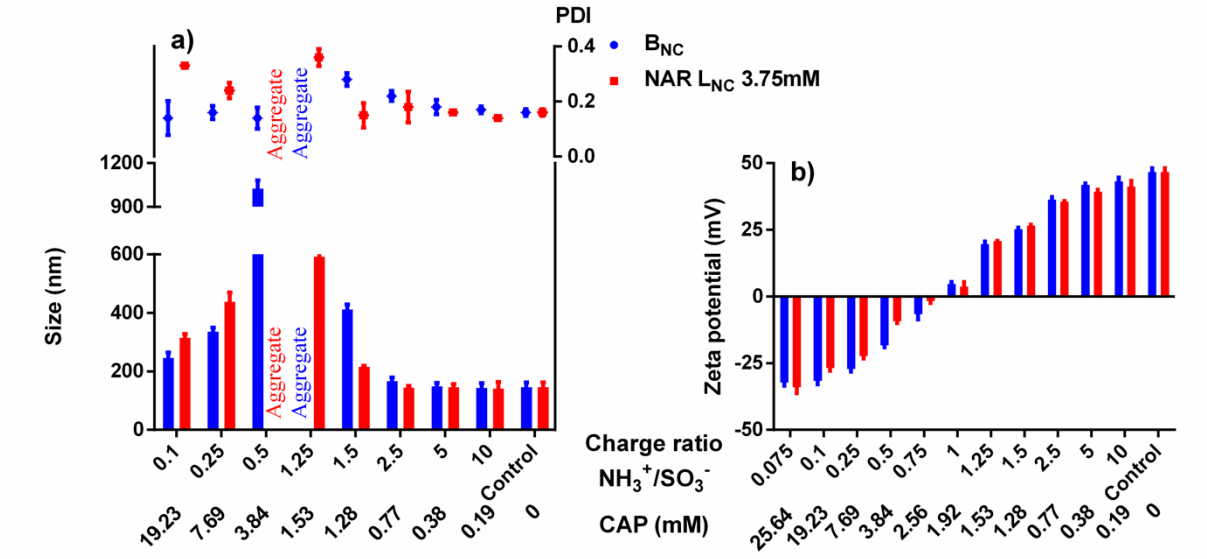


**Figure 3.** Physicochemical characteristics (A: Z-average size and PDI, B: Zeta potential) of $B_{NC}$ and NAR $L_{NC}$ 3.75mM with Captisol® adsorbed onto their surfaces. $B_{NC}$ and NAR $L_{NC}$ 3.75mM that did not undergo mixing with Captisol® were set up as the controls. As shown on the x-axis labels, the first row is the charge ratio between the amine group of chitosan and the sulfate group of Captisol® ($[NH_3^+]/[SO_3^-]$), and the second row is the equivalent amount of Captisol® in the corresponding charge ratio.

### 3.5. TEM images

In general, the physicochemical properties of a given nanosystem depend on the size distribution, ζ-potential and morphology. Transmission electron microscopy (TEM) is one of the most suitable techniques to image the microstructure morphology of nanoparticles of different type of our study (Fig. S3). Notice that all the imaged systems exhibited a spherical morphology with sizes within the range determined by DLS-NIBS (Table 1 and Fig. S3). TEM images of the nanocapsules (Fig. S3A and B) revealed a core-shell structure, including a thin surface with irregular topography. The presence of a shell structure observed in NC is not so evident in the nanoemulsions (Fig. S3C and D). In turn, the micrographs of 19 mM Captisol®-adsorbed nanocapsules (charge ratio +/- of 0.1) showed some differences (Fig. S3E and F) particularly in the thickness of the shell as it can be notice by close inspection of few of the imaged particles. We reasoned that excess amounts of Captisol® (19.23 mM) would be able to effectively associate with the cationic surface of NC and coat it completely, thus causing a significant increase in particle size consistent with the Z-average size values shown in Figure 3. By contrast, at high +/- charge ratios, when Captisol® is in defect (0.38 mM) (Fig. S3_G and H) it appears that the NC's shell thickness is similar to that of the control NC. In all the systems, it can be noticed the presence of irregularities in the topology. This may be consistent with the occurrence of patches of Captisol® complexed with chitosan.

### 3.6. QS inhibition activity of the nanosystems

We evaluated the influence of individual components (Fig. 4) and different nanoformulation (Fig. 5) on the relative growth and relative QS activity of the biosensor *E. coli* Top 10 strain, while the influence of these factors on bacterial growth ($OD_{600}$), fluorescence intensity (FL), and relative light unit ($RLU=FL/OD_{600}$) was shown in Fig. S7 and S8

Since Captisol® did not exhibit the bacterial growth at two concentrations namely 0.019 and 0.961 nM (Fig. S 7A) , but it reduced significantly fluorescence intensities (Fig. S7 B), thus displaying a significant anti-QS effect (Fig. 4b). Chitosan at 0.05 mg/mL and NAR at 0.187 mM (the same concentrations in NC systems) caused a reduction of bacterial growth by nearly 13.78 and 25.06 %, respectively (Fig. 4a).

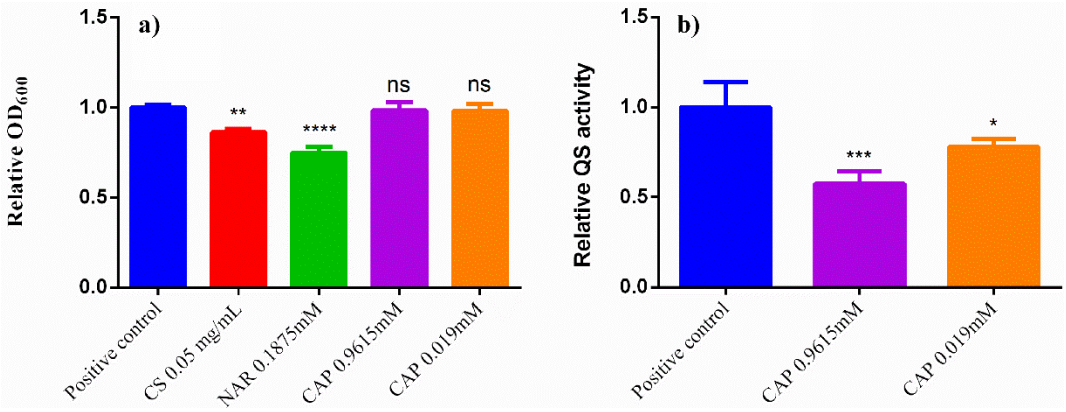

**Figure 4**. Effects of different formulations on relative bacterial growth ($OD_{600}$) and relative QS activity (a, b) after 300 min. Statistical test: one-way ANOVA, multiple comparisons with respect to the positive control: * $p < 0.05$, ** $p < 0.01$, *** $p < 0.001$**** $p < 0.0001$). Key: CAP: Captisol®, NAR: naringenin, CS: chitosan.

The influence of different nanoformulations was also evaluated under the same assay as described above (Fig. 5 and Fig. S8). Notice in Fig. S8A, both blank and NAR-loaded NC did not inhibit bacterial growth, consistent with the notion that these NC system formulations are non-toxic to bacteria.

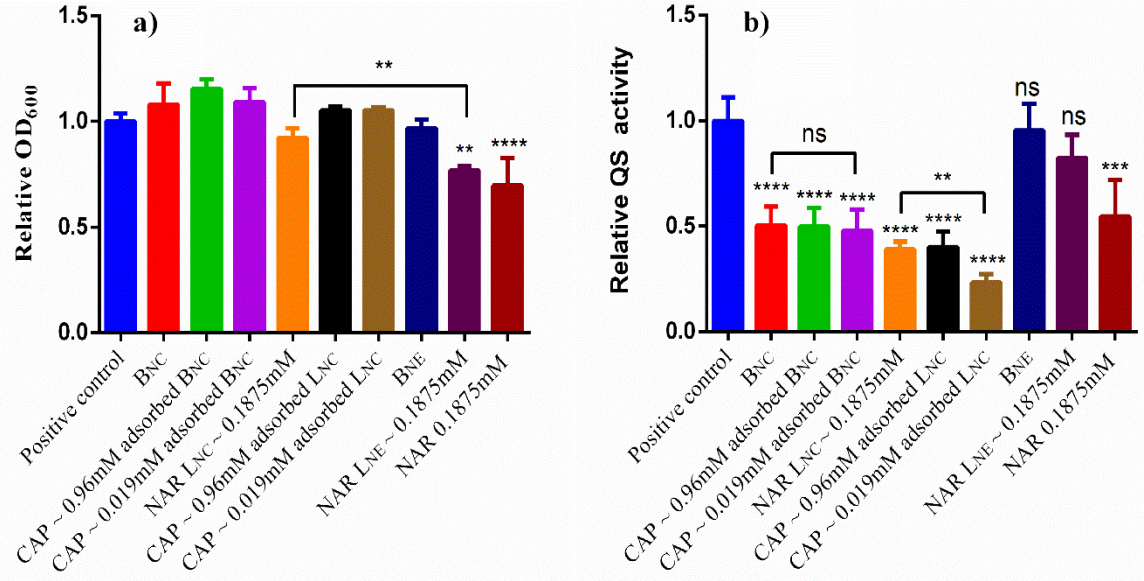


**Figure 5**. Effects of different formulations on relative bacterial growth ($OD_{600}$) and relative anti-QS activities (a, b) after 300 min. Statistical test: one-way ANOVA, multiple comparisons with respect to the positive control: * $p < 0.05$, ** $p < 0.01$, *** $p < 0.001$**** $p < 0.0001$).

In contrast, NAR-loaded NE showed a significant ($p < 0.001$) bacterial inhibition effect, since we observed a nearly ~ 33.89 % reduction in bacterial growth (Fig. 5a). Interestingly, while unloaded NE was non-toxic, NAR-loaded NE inhibited bacterial growth, thus suggesting that the toxicity effect might stem from the loaded payload. However, when loaded in nanocapsules, the toxicity seems to be reduced, thus suggesting that upon encapsulation, the toxicity of free components such as chitosan and NAR was significantly reduced (*cf.* NAR free form *vs*. loaded NE *vs*. loaded NC). Surprisingly, despite NAR-loaded NC and NAR-loaded NE contained the same amount of loaded payload and released comparable amounts of it (Fig. 2), yet they exhibited opposite effects on bacterial growth. This highlights the crucial role of the chitosan corona of the NC in reducing their toxicity.

Since Captisol® is non-toxic to bacteria (Fig. 4a), its adsorption onto NC surfaces did not change the toxicity properties of these systems (Fig. 5a). Although loaded NE formulations significantly inhibited bacterial growth, the fluorescence quenching effect was negligible. As we expected, both blank and loaded NC exhibited better fluorescence quenching effects than

NE systems, in agreement with our previous studies [11]. The highly positive surface charge of NC could explain this phenomenon, given the electrostatic interactions between the oppositely charged surfaces of NC and bacteria. Moreover, NAR-loaded NC showed more substantial anti-QS effects than NC blank formulations (*cf.* ~ 49.55 and ~ 60.89 %, respectively, Fig. 5b), thus suggesting that NAR might act synergistically with chitosan to increase the anti-QS activity. In the case of Captisol® surface-adsorbed NC (blank and NAR-loaded), the most significant fluorescence quenching effect was induced by the formulation of CAP ~ 0.019 mM adsorbed onto $B_{NC,}$ and the formulation of CAP ~ 0.019 mM adsorbed onto NAR-loaded NC ($L_{NC}$). However, only the difference between $L_{NC}$ and CAP ~ 0.019 mM adsorbed $L_{NC}$ reached a statistically significant difference (Figure 5b). Adsorption of Captisol® in CAP ~ 0.019 mM adsorbed $L_{NC}$ formulations resulted in anti-QS activities up to ~ 76.63 %, which was around 16 % higher than in the NAR-loaded NC system without surface-adsorbed Captisol®, while the nanosystem was still able to maintain a positive ζ-potential (~+40 mV, Figure 3b). The combination of a positively charged amine group, the gradual release of NAR, and Captisol®'s ability to trap autoinducers could explain why this formulation attained the best anti-QS effect. Given that electrostatic interactions between chitosan-coated nanocapsules and *E. coli* bacteria have been found to favor the anti-QS activity [11], formulations of NAR-loaded NC ($L_{NC}$) comprising the highest amounts of adsorbed Captisol® (0.96 mM), thus bearing a highly negative charged surface, exhibited significantly lower fluorescence quenching than did the loaded formulation with defect of Captisol® (CAP-0.019mM adsorbed $L_{NC}$). Based on this evidence, we venture to hypothesize that for the systems comprising the highest amounts of adsorbed Captisol®, the NAR released from the oil-core of the nanosystems is trapped inside the Captisol® cavity, thus resulting in the less strong quenching effect seen here.

### 3.7. Anti-biofilm activity of the nanosystems

We investigated the effect of free components (NAR and chitosan) and different nanoformulations on the biofilm formation in the *E. coli* Top 10 biosensor strain (Figure 6; Fig. S4 and S5). Notably, $B_{NE}$, free chitosan and free NAR exhibited negligible anti-biofilm effects by 5.11, 17.64 and 11.35 %, respectively, as compared to the positive control (kanamycin 1 mM). Interestingly, the NAR-$L_{NE}$ seemed to promote biofilm formation. In contrast, all nanocapsule formulations showed significant inhibition of biofilm formation. Of note, NAR-$L_{NC}$ showed stronger biofilm inhibition effects compared to their unloaded counterparts ($L_{NC}$ *vs.* $B_{NC}$; CAP adsorbed $L_{NC}$ *vs.* CAP adsorbed $B_{NC}$ ). Interestingly, the adsorption of Captisol® onto the surface of NC did not lead to a further increase anti-biofilm effect beyond those associated with the NC alone. In fact, the more Captisol® adsorbed to NC surfaces, the lesser the anti-biofilm effect. Anti-biofilm effects were not reduced when only a small amount of Captisol® (0.019 mM) was adsorbed to the surface of both blank and NAR-loaded nanocapsules. The highest anti-biofilm effect was obtained for the NAR-loaded $L_{NC}$ ~ 0.1875

mM formulation, reducing biofilm formation by nearly ~ 60 % (compared to the negative control), thus highlighting the synergistic anti-biofilm effects of positively charged chitosan, enhanced by the high surface area-to-volume ratio of NC, and the bioactivity of NAR.

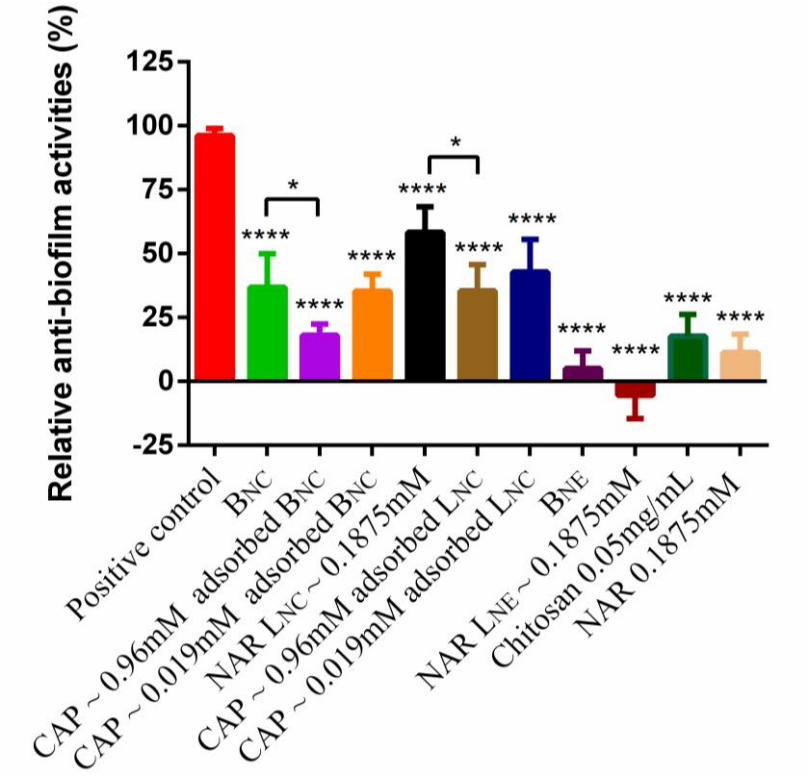


**Figure 6.** Relative anti-biofilm activities following treatment with different formulations of free components and the nanosystems. Kanamycin (1mM) was used as positive control. Mean values ± SD. Statistical test: one-way ANOVA, multiple comparisons (n = 3, * $p < 0.05$, **** $p < 0.0001$).

### 3.8. Cytotoxicity of different formulations against Caco-2 cells

The influence of different concentrations of the components and various nanoformulations on the viability of Caco-2 cells was assessed by using MTT assay. MEM medium and Triton-X 4% were used as positive and negative control, respectively.

As can be observed, except for the free NAR at the two concentrations of 0.075 and 0.1875 mM, which caused significant inhibition to cell growth, the other components of the nanosystems were non-toxic to Caco-2 cells (Fig. 7a). The free chitosan solution exerted a slight growth inhibition effect, but this effect was not statistically significant.

The cytotoxicity of nanoformulations is shown in Fig. 7b. All treatments with loaded and unloaded nanoformulations were applied at the same carrier concentrations. As can be seen, both blank and loaded NC as well as Captisol® surface-adsorbed nanosystems are non-toxic to the mammalian Caco-2 cell line, thus indicating that the encapsulation process exhibited a cytoprotective effect compared to the free payload formulations. This is in line with a previous

study, where nanoencapsulation of capsaicin was found to improve the relative viability in MDCK7 cells [28].

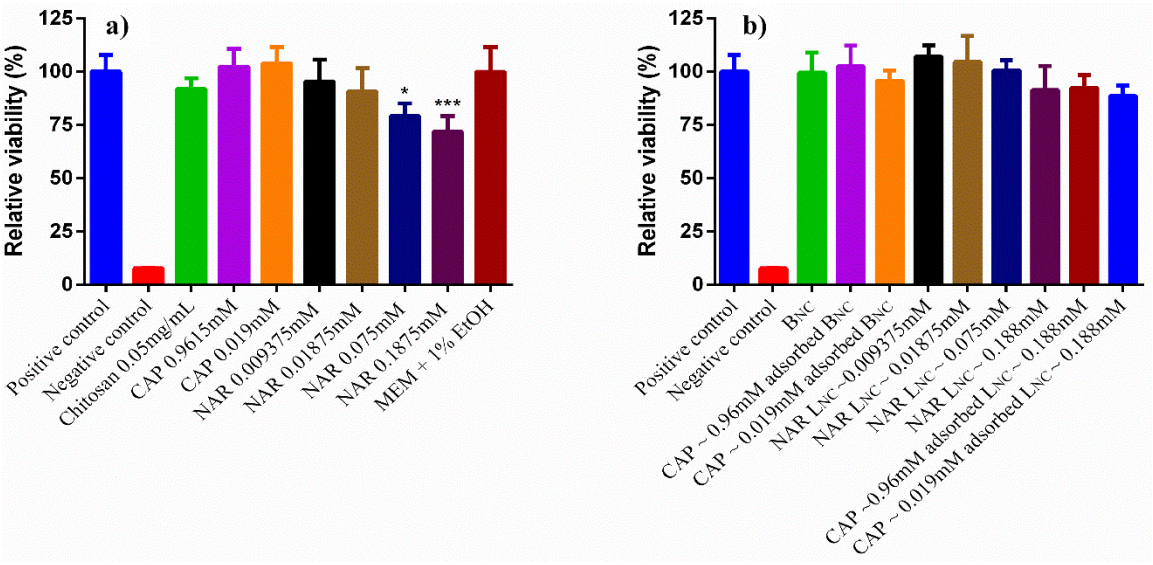


**Figure 7.** Cytotoxicity of different formulations against Caco-2 cells of individual components (a) and with the different nano-formulations (b). Mean values ± SD. Statistical test: one-way ANOVA, multiple comparisons ($n$ = 3, * $p < 0.05$, ***$p < 0.001$). Key: CAP: Captisol®, MEM: Minimum Essential Medium, EtOH: Ethanol.

## 4. Discussion

We used a combination of biophysical and biological assays to compare the ability of free NAR , NAR-loaded nanoformulations comprising an emulsified oily core stabilized by lecithin (nanoemulsions), lecithin and chitosan (nanocapsules) or a LbL of lecithin, chitosan and Captisol®, to interfere with bacteria collactive cell-cell communication, known as quorum sensing (QS), using an *E. coli* Top10 reporter strain. First, we determined the physicochemical characteristics and colloidal stability of the nanoformulations (Table 1, Fig. 1). Our results are in accordance with previous results that show that NC made of low Mw chitosan exhibited lower Z-average diameter [29]. As an expected consequence of lacking a chitosan shell, the NE size (~ 130 nm) was somewhat smaller than that of NC.

To increase the NAR-EE of the systems, we decreased the initial NAR concentration from 5 to 3.75 mM. Chitosan-coated NC retained up to ~ 92.88 % of their NAR cargo, while the NE, lacking chitosan, showed a lower NAR-EE (~ 67.98 %), thus suggesting that the presence of chitosan in the NC shells supports the retention of NAR during the emulsification process. In addition, the EE significantly increased, reaching ~ 98.81 %, when CAP (19.23 mM) was adsorbed $L_{NC}$ (data not shown). It is unsurprising that when NAR can be trapped inside the Captisol®'s cavity by creating an inclusion complex at the NC's surface, the EE increased by ~ 6 % (98.8 % in NAR $L_{NC}$ 3.75 mM *vs.* 92.8 % in CAP ~19.23 mM adsorbed NAR $L_{NC}$ 3.75 mM). In agreement with our phase solubility studies (Figure S6), 19.23 mM of Captisol® can trap up to ~1.832 mg/mL of NAR in an equilibrium condition (after incubation at 37 °C for at

least 2 days). Although the EE increased significantly in both the NE and NC nanosystems tested whilst the loading efficiencies were kept the same (~ 4 and ~ 6 % for NE and NC systems, respectively), this might suggest that these values might be the maximal loading capacity of both types of nanosystems. Hence, these results once again indicate that the chitosan shell of NC affects not only the physicochemical characteristics of a nanocarrier but also the capacity to encapsulate lipophilic drugs [29].

Our previous stability experiments have demonstrated that the hydrophilicity increased with the degree of acetylation (DA) but decreased with the molecular weight of chitosan [42]. Hence, chitosan used in this study with DA of 32 % and relatively low $M_w$ ~ 29267 g.mol$^{-1}$ is expected to result in highly stable systems. As an explanation for these phenomena, an increment in DA raises the number of hydrophobic parts in the chitosan backbone, and the attractive hydrophobic interactions between these fragments and the hydrophobic areas of the oil/lecithin particle expose the hydrophilic regions to the aqueous phase while the hydrophobic parts are hidden. In addition, lower molecular weight chitosan chains supply a more hydrophilic shell that are supposed to be re-accommodated much better on the surface – avoiding their contact with water than those parts in high molar mass chains [42].

A controlled, biphasic release of NAR was observed from both the NE and NC systems in bacterial M9 medium *in vitro* (Fig. 2). The nature of the shells in the NC and NE formulations resulted in different *in vitro* NAR release profiles. The release rate was more prolonged in the NC system, showing around 5 % of the released payload after 6 h compared to around 12 % from the NE system. The gradual release of drug by the NC can be explained by the diffusion of a small amount of drug that was strongly bound in the interface between the lecithin and the chitosan shell, while the exponential phase occurred because of the burst release of the large amount of NAR encapsulated in the oily core. This binding effect in the NC system sounds to diminish the permeability of the NAR payload from the oily core during the initial release period. The gradual dissociation of the chitosan-phospholipid complex in M9 medium might contribute to the duration of the second exponential stage, which also suggests that chitosan plays a vital role in driving a prolonged and sustained release of NAR. The sustained release will in turn, limit the side effects due to reduce the drug's dosage, improve a drug's bioavailability and prolong activity at the targeted site [43].

We found that both anti-QS and anti-biofilm activities increased significantly upon using NC. This highlights the benefit of unique physicochemical properties and the high surface area-to-volume ratio of nanoparticles that facilitate their attachment to bacterial membranes, enhance the bioactivities of these systems and limit their toxicity. As evidenced in Fig. 5, the greatest anti-QS effect was attained in the formulation of CAP 0.019 mM adsorbed $L_{NC}$, suggesting that combination of the release of NAR from the NC oily core and the simultaneous uptake of 3OC6HSL inside Captisol®'s cavity could be the reason for enhanced anti-QS and anti-biofilm activities. However, increasing the amount of Captisol® adhered to NC to 0.96 mM did not

further enhance these effects; in fact, higher GFP production was observed in both "CAP 0.96 mM adsorbed $L_{NC}$" and "CAP 0.96 mM adsorbed $B_{NC}$" formulations compared to their $L_{NC}$ and $B_{NC}$ counterparts, respectively. Since electrostatic interactions favor anti-QS effects, the highly negative surface charge in these CAP 0.96 mM formulations made it difficult for them to deliver the released drug at the target site. Therefore, any GFP reduction seen for those formulations may have only been due to the amount of AHL they were able to entrap in the Captisol's cavity, not NAR drug release.

QS inhibitors function by targeting one of the following processes involved in QS: inactivation of the signal molecules, inhibition of the signal receptors, or inhibition of the signal biosynthesis [44]. Given that our biosensor does not possess the autoinducer synthase machinery (luxI), we cannot speculate that NAR inhibited the signal biosynthesis. As QS circuits in *P. aeruginosa* and *E. coli* Top 10 respond to different types of autoinducers, and NAR exerts anti-QS effects on both systems [22], we can also exclude the possibility that NAR competed with the cognate autoinducers for binding sites on the involved receptors. An alternative explanation is that NAR might be accumulated rapidly in the lipidic bacterial membrane, causing it to block the diffusion of AHL to the cytosol. This mechanism seems to be the most plausible, as it can explain why free NAR is highly toxic to bacterial growth in a dose dependent manner while NC are not. First, the anti-QS activity of the NC might be enhanced as a result of the NC's strong positive charge, which promotes binding with the bacterial membrane [11]. This may allow the NC to deliver their payloads locally at the bacterial cell wall whilst maintaining a lower overall NAR dose for the duration of the experiment, thereby prolonging anti-QS effects. Furthermore, the NC system releases NAR in a sustained manner, thus providing time for bacteria to adapt to and metabolize the drug. Adsorption of Captisol® at the NC surface might then enable the "abduction" of AHL, leading to inactivation of this autoinducer. Overall, our results are in accordance with previous studies [45–47] that have suggested autoinducers, in particular AHLs which possess an acyl chain from C4 to C8 may be trapped inside the Captisol® cavity, thus leading to the reduction in QS activity.

According to a previous study, the geometry of a surface can determine the initial location of adhering cells, whereby bacterial cells preferentially adhere to square corners and convex walls rather than flat surfaces [48]. Therefore, in this study, we conducted our experiments in "U bottom shaped" plates. We chose crystal violet, a cationic dye that non-specifically stains negatively charged biofilm via ionic interactions [49], to quantify the biofilm formation in different formulations. Biofilm is one of the most common processes activated by communities of bacteria in a cooperative manner. In many cases, biofilm formation significantly increases pathogenic bacteria's tolerance for normal antibiotics, making them more and more useless. Biofilm formation is known to be a QS-dependent process in many bacterial species [50–52], but the precise mechanism and stage in biofilm formation/regulation mediated by QS is still

not fully elucidated (Supplementary Information 3.1 ). In this study, we interrupted QS by blocking the diffusion of an autoinducer driven by the opposite charges of the bacterial membrane and the NC surfaces; as a result, biofilm formation was significantly reduced. Notably, chitosan and NAR existing in free form did not exhibit any statistically significant anti-biofilm effects, and neither did the NAR-loaded nanoemulsion system. However, when a nanocapsule-based system was used, both with and without drug loading, it was able to significantly quench biofilm formation in our biosensor, thus indicating the unique ability of nanocapsule systems to bind to the bacterial cell envelope and therefore prevent them from forming microcolonies. Of note, the anti-biofilm effects were greatest in NAR-$L_{NC}$ formulations, suggesting that chitosan and NAR might act on different targets in optimizing the anti-biofilm effect and probably acting in synergy on such mechanisms.

As a natural QS inhibitor, NAR has several advantages. First, NAR is low in cost and abundant in nature. Second, NAR was harmless upon exposure to rat gastrointestinal epithelium at a concentration of 100 mM [53]. Third, besides its anti-QS effects, NAR has recently been reported to augment anticancer activity against MCF-7 human breast cancer cells [54] and to inhibit the tumor growth on different human cancer cell lines such as MCF-7, Hela, and Caco-2 cells [55]. In this study, NAR administered as a free solution was found to reduce the viability of human colon cancer Caco-2 cells under a dose-response profile. However, this effect was not observed when NAR was encapsulated and dosed identically as in the free form, thus reflecting a cytoprotective effect of the NC against mammalian cells. Whether the same NC formulation could be used concomitantly to enhance bacterial anti-QS, prevent biofilm formation, and be co-loaded with other known agents (e.g. curcumin) to help in reducing proliferation of carcinogenic tumor cells, is to be established in future studies.

## 5. Conclusions

In summary, herein we have developed a novel nanosystem that involves incorporating quorum sensing inhibitors within multifunctional nanocapsules to be used as quorum quenching compounds. Chitosan-based NC appear to be a promising candidate for delivering their payloads target on the bacterial cell wall, releasing the loaded drug in a sustained and controlled manner and thereby enhancing and prolonging their anti-QS and anti-biofilm activities. The adsorption of 0.19 mM Captisol® on NAR $L_{NC}$ led to increase anti-QS up to ~ 16 %. Another favorable effect of encapsulating the NAR flavonoid was the cytoprotective effect on Caco-2 cells. Since QS is responsible for biofilm formation for many microbes, therapeutic strategies targeting QS systems are promising for the development of drugs that can replace traditional antibiotics. Nonetheless, the precise mechanisms underlying how QS mediates biofilm formation still needs to be fully elucidated. The results of the current study will need to be validated in *in vivo* in future studies. Future studies could also explore co-loading flavonoids along with other bioactive payloads and surfactants into the same nanocapsule formulations to achieve higher bioactive (may be synergistic) effects.

## Acknowledgement

The authors would like to thank Dr. Cleste Brennecka (Language Center, Bispinghof 2B, 48143 Münster) and Rossie Owen for their English editing support. The help of Mr. Harald Nüsse (Institut für Medizinische Physik und Biophysik, UKM Münster) with TEM images analysis is also highly appreciated. We are indebted to Celina Vila for providing the *E. coli* Top 10 QS strain.

# References

1. Clatworthy, A.E.; Pierson, E.; Hung, D.T. Targeting virulence: a new paradigm for antimicrobial therapy. *Nat. Chem. Biol.* **2007**, *3*, 541–548.
2. Frost, K.J. An overview of antibiotic therapy. *Nurs. Stand.* **2007**, *22*, 51–7; quiz 58.
3. Appelbaum, P.C. 2012 and beyond: Potential for the start of a second pre-antibiotic era? *J. Antimicrob. Chemother.* **2012**, *67*, 2062–2068.
4. Dopazo, C.P.; Lemos, M.L.; Lodeiros, C.; Bolinches, J.; Barja, J.L.; Toranzo, A.E. Inhibitory activity of antibiotic-producing marine bacteria against fish pathogens. *J. Appl. Bacteriol.* **1988**, *65*, 97–101.
5. Ng, W.-L.; Bassler, B.L. Bacterial Quorum-Sensing Network Architectures. *Annu. Rev. Genet* **2009**, *43*, 197–222.
6. Waters, C.M.; Bassler, B.L. Quorum Sensing: Cell-to-Cell Communication in Bacteria. *Annu. Rev. Cell Dev. Biol* **2005**, *21*, 319–346.
7. Henke, J.M.; Bassler, B.L. Three Parallel Quorum-Sensing Systems Regulate Gene Expression in Vibrio harveyi. *J. Bacteriol.* **2004**, *186*, 6902–6914.
8. Kumar, S.; Costantino, V.; Venturi, V.; Steindler, L. Quorum sensing inhibitors from the sea discovered using bacterial N-acyl-homoserine lactone-based biosensors. *Mar. Drugs* **2017**, *15*.
9. Hawver, L.A.; Jung, S.A.; Ng, W.L. Specificity and complexity in bacterial quorum-sensing systemsa. *FEMS Microbiol. Rev.* **2016**, *40*, 738–752.
10. Thanh Nguyen, H.; Goycoolea, F.M. Chitosan/Cyclodextrin/TPP Nanoparticles Loaded with Quercetin as Novel Bacterial Quorum Sensing Inhibitors. *Molecules* **2017**, *22*, 1975.
11. Qin, X.; Engwer, C.; Desai, S.; Vila-Sanjurjo, C.; Goycoolea, F.M. An investigation of the interactions between an *E. coli* bacterial quorum sensing biosensor and chitosan-based nanocapsules. *Colloids Surfaces B Biointerfaces* **2017**, *149*, 358–368.
12. Omwenga, E.O.; Hensel, A.; Shitandi, A.; Goycoolea, F.M. Chitosan nanoencapsulation of flavonoids enhances their quorum sensing and biofilm formation inhibitory activities against an E.coli Top 10 biosensor. *Colloids Surfaces B Biointerfaces* **2018**, *164*, 125–133.
13. Engebrecht, J.; Nealson, K.; Silverman, M. Bacterial bioluminescence: Isolation and genetic analysis of functions from Vibrio fischeri. *Cell* **1983**, *32*, 773–781.
14. Tang, K.; Zhang, X.H. Quorum quenching agents: Resources for antivirulence therapy. *Mar. Drugs* **2014**, *12*, 3245–3282.
15. Romero, M.; Diggle, S.P.; Heeb, S.; Amara, M.; Otero, A. Quorum quenching activity in Anabaena sp. PCC 7120: identi¢cation of AiiC, a novel AHL-acylase. *FEMS Microbiol Lett* **2008**, *280*, 73–80.
16. Truchado, P.; Larrosa, M.; Castro-Ibáñez, I.; Allende, A. Plant food extracts and phytochemicals: Their role as Quorum Sensing Inhibitors. *Trends Food Sci. Technol.* **2015**, *43*, 189–204.
17. Girennavar, B.; Cepeda, M.L.; Soni, K.A.; Vikram, A.; Jesudhasan, P.; Jayaprakasha, G.K.; Pillai, S.D.; Patil, B.S. Grapefruit juice and its furocoumarins inhibits autoinducer signaling and biofilm formation in bacteria. *Int. J. Food Microbiol.* **2008**, *125*, 204–8.
18. Vikram, A.; Jesudhasan, P.R.; Jayaprakasha, G.K.; Pillai, S.D.; Patil, B.S. Citrus limonoids interfere with Vibrio harveyi cell-cell signalling and biofilm formation by modulating the response regulator luxO. *Microbiology* **2011**, *157*, 99–110.
19. Teasdale, M.E.; Donovan, K.A.; Forschner-Dancause, S.R.; Rowley, D.C. Gram-Positive Marine Bacteria as a

Potential Resource for the Discovery of Quorum Sensing Inhibitors. *Mar. Biotechnol.* **2011**, *13*, 722–732.

20. Sedef Ilka, Necdet Sa˘glam, Mustafa Özgen, F.K. Chitosan nanoparticles enhances the anti-quorum sensing activity of kaempferol. *Int. J. Biol. Macromol.* **2017**, *94*, 653–662.

21. Defoirdt, T.; Boon, N.; Sorgeloos, P.; Verstraete, W.; Bossier, P. Quorum sensing and quorum quenching in Vibrio harveyi: lessons learned from in vivo work. *ISME J.* **2008**, *2*, 19–26.

22. Vandeputte, O.M.; Kiendrebeogo, M.; Rasamiravaka, T.; Stévigny, C.; Duez, P.; Rajaonson, S.; Diallo, B.; Mol, A.; Baucher, M.; el Jaziri, M. The flavanone naringenin reduces the production of quorum sensing-controlled virulence factors in pseudomonas aeruginosa PAO1. *Microbiology* **2011**, *157*, 2120–2132.

23. Niu, C.; Afre, S.; Gilbert, E.S. Subinhibitory concentrations of cinnamaldehyde interfere with quorum sensing. *Lett. Appl. Microbiol.* **2006**, *43*, 489–494.

24. Gupta, A.; Kaur, C.D.; Saraf, S.; Saraf, S. Formulation, characterization, and evaluation of ligand-conjugated biodegradable quercetin nanoparticles for active targeting. *Artif. cells, nanomedicine, Biotechnol.* **2016**, *44*, 960–970.

25. Qin, X.; Kräft, T.; Goycoolea, F.M. Chitosan encapsulation modulates the effect of trans -cinnamaldehyde on AHL-regulated quorum sensing activity. *Colloids Surfaces B Biointerfaces* **2018**, *169*, 453–461.

26. Torchilin, V.P. Multifunctional nanocarriers. *Adv. Drug Deliv. Rev.* **2012**, *64*, 302–315.

27. Manju RAWAT, Deependra SINGH, S. SARAF, and S.S. Nanocarriers: Promising Vehicle for Bioactive Drugs. *Biol. Pharm. Bull.* **2006**, *29*, 1790–1798.

28. Kaiser, M.; Pereira, S.; Pohl, L.; Ketelhut, S.; Kemper, B.; Gorzelanny, C.; Galla, H.-J.; Moerschbacher, B.M.; Goycoolea, F.M. Chitosan encapsulation modulates the effect of capsaicin on the tight junctions of MDCK cells. *Sci. Rep.* **2015**, *5*, 10048.

29. Goycoolea, F.M.; Valle-Gallego, A.; Stefani, R.; Menchicchi, B.; David, L.; Rochas, C.; Santander-Ortega, M.J.; Alonso, M.J. Chitosan-based nanocapsules: Physical characterization, stability in biological media and capsaicin encapsulation. *Colloid Polym. Sci.* **2012**, *290*, 1423–1434.

30. Ho, P.C.; Saville, D.J.; Coville, P.F.; Wanwimolruk, S. Content of CYP3A4 inhibitors, naringin, naringenin and bergapten in grapefruit and grapefruit juice products. *Pharm. Acta Helv.* **2000**, *74*, 379–385.

31. Gel-Moreto, N.; Streich, R.; Galensa, R. Chiral separation of diastereomeric flavanone-7-O-glycosides in citrus by capillary electrophoresis. *Electrophoresis* **2003**, *24*, 2716–2722.

32. Olsen, H.T.; Stafford, G.I.; van Staden, J.; Christensen, S.B.; Jäger, A.K. Isolation of the MAO-inhibitor naringenin from Mentha aquatica L. *J. Ethnopharmacol.* **2008**.

33. Vikram, A.; Jayaprakasha, G.K.; Jesudhasan, P.R.; Pillai, S.D.; Patil, B.S. Suppression of bacterial cell-cell signalling, biofilm formation and type III secretion system by citrus flavonoids. *J. Appl. Microbiol.* **2010**, *109*, 515–527.

34. Shulman, M.; Cohen, M.; Soto-Gutierrez, A.; Yagi, H.; Wang, H.; Goldwasser, J.; Lee-Parsons, C.W.; Benny-Ratsaby, O.; Yarmush, M.L.; Nahmias, Y.; et al. Enhancement of Naringenin Bioavailability by Complexation with Hydroxypropoyl-b-Cyclodextrin. *PLoS One* **2011**, *6*, 1–8.

35. Calixto, G.; Fonseca-Santos, B.; Chorilli, M.; Bernegossi, J. Nanotechnology-based drug delivery systems for treatment of oral cancer: a review. *Int. J. Nanomedicine* **2014**, *9*, 3719–3735.

36. Praveen Kumar, S.; Birundha, K.; Kaveri, K.; Ramya Devi, K. Antioxidant studies of chitosan nanoparticles containing naringenin and their cytotoxicity effects in lung cancer cells. *Int. J. Biol. Macromol.* **2015**, *78*, 87–95.

37. Gonzalez-Espinosa Y., Sabagh B., Moldenhauer E., Clarke P, F.M.G. Characterisation of Chitosan Molecular Weight Distribution by Multidetection Asymmetric Field-Flow Fractionation and SEC-MALS (submitted). *Int. J. Biol. Macromol.*

38. Calvo, P.; Remunan-Lopez, C. Development of positively charged colloidal drug carriers:chitosan-coated polyester nanocapsules and submicron-emulsions. *Colloid Polym. Sci.* **1997**, *275*, 46–53.

39. Denizot, F.; Lang, R. Rapid colorimetric assay for cell growth and survival. *J. Immunol. Methods* **1986**, *89*, 271–277.

40. O'Toole, G.A. Microtiter Dish Biofilm Formation Assay. *J. Vis. Exp.* **2011**, *47*.

41. Lozano, M. V.; Torrecilla, D.; Torres, D.; Vidal, A.; Domínguez, F.; Alonso, M.J. Highly efficient system to deliver taxanes into tumor cells: Docetaxel-loaded chitosan oligomer colloidal carriers. *Biomacromolecules* **2008**, *9*, 2186–

2193.

42. Santander-Ortega, M.J.; Peula-García, J.M.; Goycoolea, F.M.; Ortega-Vinuesa, J.L. Chitosan nanocapsules: Effect of chitosan molecular weight and acetylation degree on electrokinetic behaviour and colloidal stability. *Colloids Surfaces B Biointerfaces* **2011**, *82*, 571–580.

43. Dozie-Nwachukwu, S.O.; Danyuo, Y.; Obayemi, J.D.; Odusanya, O.S.; Malatesta, K.; Soboyejo, W.O. Extraction and encapsulation of prodigiosin in chitosan microspheres for targeted drug delivery. *Mater. Sci. Eng.* **2017**, *C 71*, 268–278.

44. Fetzner, S. Quorum quenching enzymes. *J. Biotechnol.* **2014**, *201*, 2–14.

45. Brackman, G.; Garcia-Fernandez, M.J.; Lenoir, J.; De Meyer, L.; Remon, J.-P.; De Beer, T.; Concheiro, A.; Alvarez-Lorenzo, C.; Coenye, T. Dressings Loaded with Cyclodextrin-Hamamelitannin Complexes Increase Staphylococcus aureus Susceptibility Toward Antibiotics Both in Single as well as in Mixed Biofilm Communities. *Macromol. Biosci.* **2016**, *16*, 859–869.

46. Nasuno, E.; Umemura, T.; Ogi, T.; Okano, C.; Kawanago, T.; Iimura, K.; Morohoshi, T.; Ikeda, T.; Kato, N. Inhibitory Effects of Quorum Sensing in Serratia marcescens AS-1 by Electrospun Polyvinyl Alcohol Fibers Immobilized with Cyclodextrin. *Trans. Mater. Res. Soc. Japan* **2012**, *37*, 593–596.

47. Morohoshi, T.; Tokita, K.; Ito, S.; Saito, Y.; Maeda, S.; Kato, N.; Ikeda, T. Inhibition of quorum sensing in gram-negative bacteria by alkylamine-modified cyclodextrins. *J. Biosci. Bioeng.* **2013**, *116*, 175–179.

48. Vadillo-Rodríguez, V.; Guerra-García-Mora, A.I.; Perera-Costa, D.; Gónzalez-Martín, M.L.; Fernández-Calderón, M.C. Bacterial response to spatially organized microtopographic surface patterns with nanometer scale roughness. *Colloids Surfaces B Biointerfaces* **2018**, *169*, 340–347.

49. Christensen, G.D.; Simpson, W.A.; Younger, J.J.; Baddour, L.M.; Barrett, F.F.; Melton, D.M.; Beachey, E.H. Adherence of Coagulase-Negative Staphylococci to Plastic Tissue Culture Plates: a Quantitative Model for the Adherence of Staphylococci to Medical Devices. *J. Clin. Microbiol.* **1985**, *22*, 996–1006.

50. Rehman, Z.U.; Leiknes, T. Quorum-Quenching Bacteria Isolated From Red Sea Sediments Reduce Biofilm Formation by Pseudomonas aeruginosa. *Front. Microbiol.* **2018**, *9*, 1354.

51. Kadirvel, M.; Fanimarvasti, F.; Forbes, S.; McBain, A.; Gardiner, J.M.; Brown, G.D.; Freeman, S. Inhibition of quorum sensing and biofilm formation in Vibrio harveyi by 4-fluoro-DPD; a novel potent inhibitor of signalling. *Chem. Commun. (Camb).* **2014**, *50*, 5000–2.

52. Teschler, J.K.; Zamorano-Sánchez, D.; Utada, A.S.; Warner, C.J.A.; Wong, G.C.L.; Linington, R.G.; Yildiz, F.H. Living in the matrix: assembly and control of Vibrio cholerae biofilms. *Nat. Rev. Microbiol.* **2015**, *13*, 255–68.

53. Surampalli, G.; Nanjwade, B.K.; Patil, P.A. Safety evaluation of naringenin upon experimental exposure on rat gastrointestinal epithelium for novel optimal drug delivery. *Drug Deliv.* **2016**, *23*, 512–24.

54. Rajamani, S.; Radhakrishnan, A.; Sengodan, T.; Thangavelu, S. Augmented Anticancer Activity of Naringenin-loaded TPGS Polymeric Nanosuspension for Drug Resistive MCF-7 Human Breast Cancer Cells. *Drug Dev. Ind. Pharm.* **2018**, 1–32.

55. Kanno, S.; Tomizawa, A.; Hiura, T.; Osanai, Y.; Shouji, A.; Ujibe, M.; Ohtake, T.; Kimura, K.; Ishikawa, M. Inhibitory Effects of Naringenin on Tumor Growth in Human Cancer Cell Lines and Sarcoma S-180-Implanted Mice. *Biol. Pharm. Bull.* **2005**, *28*, 527–530.